ECCOMAS Congress 2016
VII European Congress on Computational Methods in Applied Sciences and Engineering
M. Papadrakakis, V. Papadopoulos, G. Stefanou, V. Plevris (eds.)
Crete Island, Greece, 5–10 June 2016

DUCTILE FRACTURE CRITERIA IN PREDICTION OF SLANT FRACTURE

P. Kubík[1], **F. Šebek**[1], **and J. Petruška**[1]

[1]Brno University of Technology, Faculty of Mechanical Engineering, Institute of Solids Mechanics, Mechatronics and Biomechanics, Technická 2896/2, 616 69 Brno, Czech Republic
e-mail: {kubik.p,sebek,petruska}@fme.vutbr.cz

Keywords: Ductile fracture, Coupled models, Continuum damage mechanics, Slant fracture, Localization, Explicit dynamics.

Abstract. *The ductile fracture of metallic materials is consequence of damage accumulation after straining accompanied by large plastic deformations. It is significantly dependent on the microstructure of particular material and micromechanical defects as vacancies or second phase particles. The nucleation, growth and coalescence of voids is the fracture mechanism which applies in high values of stress triaxiality. The shear mechanism appears in the region of negative stress triaxialities. Finally, the combination of both fracture mechanisms occurs in cases of moderate stress triaxialities. The crack or fracture surface in specimens or real components is often tilted approximately 45 degrees to applied load. This slant fracture is driven by shear mechanism and occurs in the plane of maximum shear stress. It was shown that coupled ductile fracture criteria are convenient for the prediction of slant fracture in finite element simulations. There is conducted analysis of slant fracture prediction ability of two chosen coupled and uncoupled criteria in the present paper. Those criteria were calibrated and applied to two different metallic materials. The prediction is validated on those calibration fracture tests at which the slant fracture was observed.*

1 INTRODUCTION

There has been a large increase of application of ductile fracture criteria to prediction of failure at various crashes and manufacturing operations as turning, cutting or cold working [1, 2, 3, 4] in the last decade due to evolution of computer technology. There are many criteria in the literature based on different approaches. Those can be simply categorized as coupled and uncoupled. Coupled criteria have mutually connected the damage with plasticity. The damage is estimated on the basis of accumulated plastic deformation and fracture strain which is dependent on the stress state. In case of uncoupled criteria, the damage is estimated by the same means but it does not influence the plasticity. The slant fracture has been still studied intensively. Huang and Xue [5] paid attention to prediction of slant ductile fracture on flat specimen, thick-walled pipe and four-point bending of a pre-cracked pipe. Morgeneyer and Besson [6] used a Gurson-like model with suggesting a shear void nucleation term based on a Lode parameter for strain rate for simulation of a fully meshed Kahn tear test sample for which a flat to slant crack transition was achieved at loads close to experimental results for aluminium. Li and Wierzbicki [7] simulated a slant fracture of a flat tensile specimens cut from advanced high strength steel sheets using partially coupled model.

The present paper deals with prediction ability of two coupled and uncoupled ductile fracture criteria on the flat specimen loaded by tension and on the smooth cylindrical specimen of Aluminium Alloy (AA) 2024 and AISI 1045 carbon steel, respectively. The most influencing parameters, mesh size and its configuration, which trigger the slant fracture were analysed. The crack initiation and propagation were realized through element deletion technique which requires the adequately small size of finite elements in principle. The numerical simulations are conducted within Abaqus/Explicit commercial finite element code with the use of user subroutine VUMAT for implementation of ductile fracture criteria into time integration scheme.

2 MODEL OF PLASTICITY AND FAILURE

2.1 Plasticity model

Isotropic hardening and von Mises yield criterion with associated flow rule were adopted. Flow curves were calibrated using tensile tests of smooth cylindrical specimens for both metals.

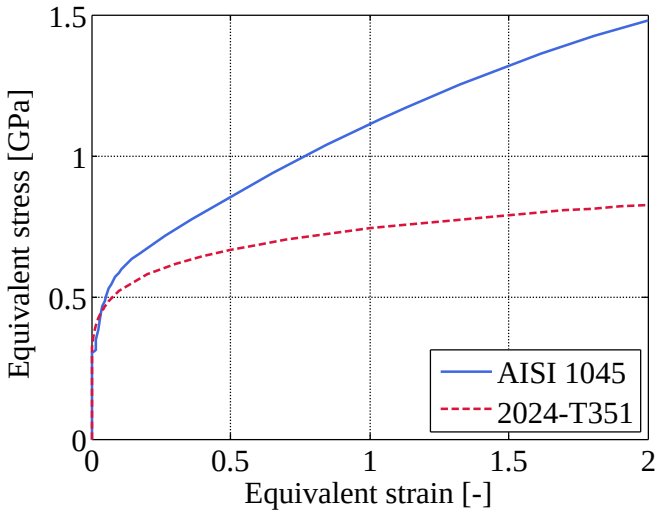

Figure 1: Flow curves of investigated metals.

Six specimens were tested having 6 mm in diameter with 30 mm gauge length of AISI 1045 steel. The flow curve until ultimate tensile strength was estimated using classical transformation formulae for true stress–strain relationship to engineering stress–strain. It is suitable to use some of correction formulae for extracting the flow curve directly from experiment beyond the plastic instability when available [8, 9, 10]. Only the elongation was measured during tensile testing in our case. Therefore, the trial and error method together with computational simulations were employed in order to change the extrapolated trend of flow curve until the satisfying match between computation and experiment was reached. Wierzbicki et al. [11] carried out a series counting fifteen experiments in a broad range of stress triaxiality η and normalized third invariant of deviatoric stress tensor ξ for AA 2024-T351. Smooth cylindrical specimen used for calibration of flow curve had 9 mm in diameter and gauge lenght of 25.4 mm. Flow curves of both materials are depicted in Fig. 1. Satisfying power law fit of those curves gave strength coefficients and strain hardening exponents summarized in Tab. 1. Hollomon hardening law, $\bar{\sigma} = K\bar{\epsilon}^n$ where $\bar{\sigma}$ is equivalent stress, K is strength coefficient, $\bar{\epsilon}$ is equivalent strain and n is strain hardening exponent, was used.

Material	Strength coefficient [MPa]	Strain hardening exponent [-]
AISI 1045	1147.6	0.2998
2024-T351	744	0.153

Table 1: Strength coefficients and strain hardening exponent of investigated materials.

2.2 Fracture criteria

Two phenomenological models were chosen in the present study. One of them was 4-parametric Xue–Wierzbicki model [11] with material constants $F_1, \ldots, F_4$ which incorporates fracture envelope $\bar{\epsilon}^f$ symmetric with respect to plane strain condition

$$\bar{\epsilon}^f(\eta, \xi) = F_1 \mathrm{e}^{-F_2\eta} - \left(F_1 \mathrm{e}^{-F_2\eta} - F_3 \mathrm{e}^{-F_4\eta}\right)\left(1 - |\xi|^{\frac{1}{n}}\right)^n \tag{1}$$

This model captures the transition between uniaxial tension and compression, where the material exhibits the greatest ductility, very well.

Another model was Extended Mohr–Coulomb criterion which was proposed by Bai and Wierzbicki [12] with the use of plasticity developed earlier [13]. The criterion contains eight material constants but only two of them, c_1 and c_2, are related to fracture. Other constants are related to Lode and pressure dependent plasticity used in the model development. When only von Mises yield criterion and Hollomon hardening law are adopted, the fracture envelope reads

$$\bar{\epsilon}^f(\eta, \bar{\theta}) = \left[\frac{K}{c_2}\left(\sqrt{\frac{1+c_1^2}{3}}\cos\left(\frac{\pi}{6}\bar{\theta}\right) + c_1\left[\eta + \frac{1}{3}\sin\left(\frac{\pi}{6}\bar{\theta}\right)\right]\right)\right]^{-\frac{1}{n}} \tag{2}$$

Deviatoric stress state parameter is the normalized Lode angle $\bar{\theta}$ here. Extended Mohr–Coulomb criterion in the presented reduced form has lower versatility than Xue–Wierzbicki model described above. It implies that it has worse approximation ability to experimental fracture tests in the calibration stage. On the other hand, the Extended Mohr–Coulomb criterion contains cut-off region dependent on the material constant c_1. Limiting stress triaxiality is described as

$$\eta_c = -\frac{1}{c_1}\left[\sqrt{\frac{1+c_1^2}{3}}\cos\left(\frac{\pi}{6}\bar{\theta}\right)\right] - \frac{1}{3}\sin\left(\frac{\pi}{6}\bar{\theta}\right) \tag{3}$$

Besides tensile test of smooth cylindrical specimen, tensile tests of notched cylindrical specimens with notch radii 5, 2.5 and 1.2 mm were included in fracture criteria calibration regarding the AISI 1045 carbon steel. The diameters in the smallest cross-section were the same as in smooth specimen. Then, biaxial tests of notched tube specimens were used in the calibration as well. Various combinations of tension–torsion loading were chosen, 0, 0.5, 1, ∞ mm/rad [14]. Comparison of force and torque responses from experiments and computations can be found in the work of Šebek et al. [15, 16].

All fifteen tests carried out by Wierzbicki et al. [11] were used for ductile fracture calibration regarding the aluminium alloy 2024-T351. More detailed information about the specimens geometry and experiment conditions can be found in the work of Bao [17].

Material constants were identified using nonlinear least square method in MATLAB. Obtained constants for both metals are summarized in Tab. 2. Fracture envelopes of particular criteria are depicted using these constants in Figs. 2 and 3. The fracture strain of both criteria is also depicted under condition of plane stress for both investigated materials in Fig. 4.

Material	Fracture criterion	Material constants
AISI 1045	Xue–Wierzbicki model	$F_1 = 3.1288$, $F_2 = 2.1351$, $F_3 = 1.2822$, $F_4 = 1.1160$
	Extended Mohr–Coulomb criterion	$c_1 = 0.2499$, $c_2 = 753.8\,\mathrm{MPa}$
2024-T351	Xue–Wierzbicki model	$F_1 = 0.7161$, $F_2 = 1.5768$, $F_3 = 0.3297$, $F_4 = 0.5232$
	Extended Mohr–Coulomb criterion	$c_1 = 0.0621$, $c_2 = 343.8\,\mathrm{MPa}$

Table 2: Material constants of both investigated materials for both criteria.

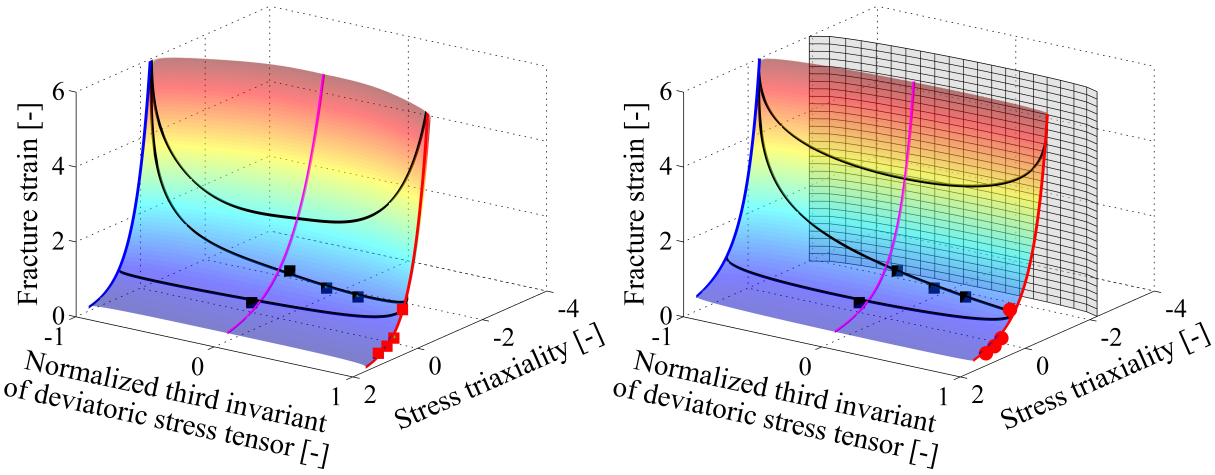

Figure 2: Fracture envelope for steel and Xue–Wierzbicki model (left), Extended Mohr–Coulomb criterion (right).

There is depicted a cut-off plane for Extended Mohr–Coulomb criterion and AISI 1045 carbon steel in Fig. 2. There is no damage accumulation below this region. There is not a cut-off plane at Extended Mohr–Coulomb criterion for aluminium alloy in Fig. 3 because it is situated in extremely low stress triaxialities, approximately -8, which is probably unrealistic.

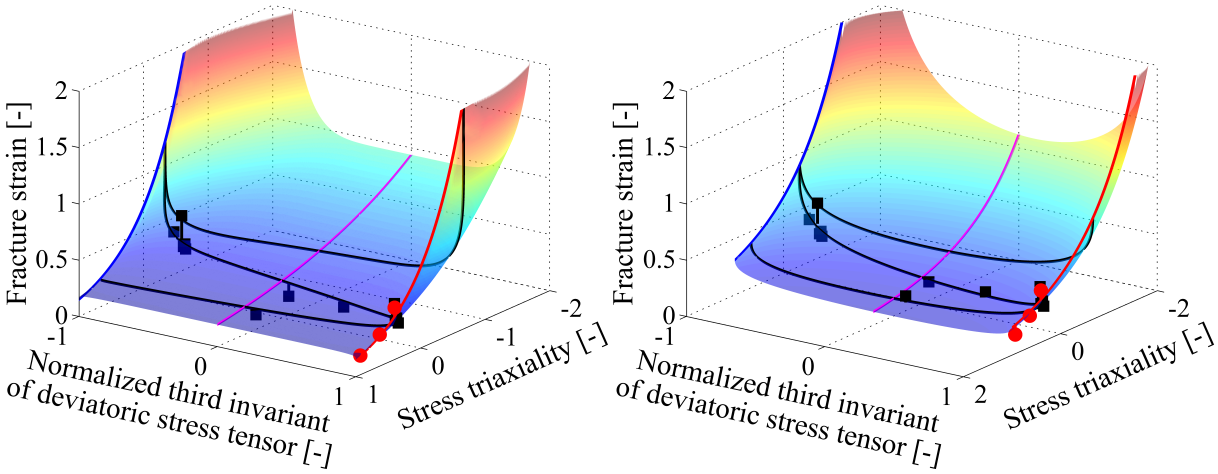

Figure 3: Fracture envelope for AA and Xue–Wierzbicki model (left), Extended Mohr–Coulomb criterion (right).

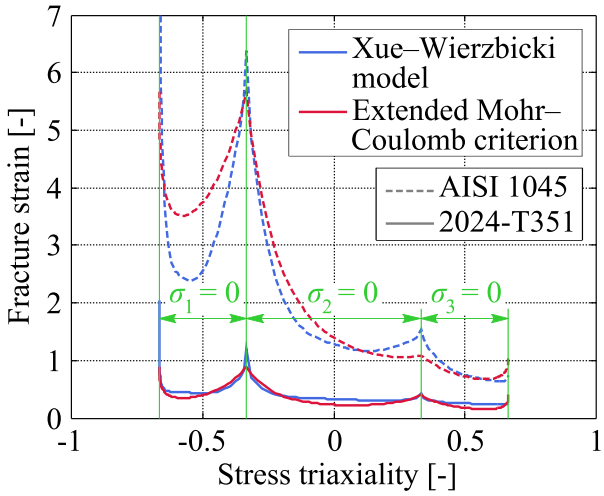

Figure 4: Fracture strain under plane stress condition for both metals.

2.3 Coupling failure with plasticity

The damage accumulation was governed by power law function derived by Xue [18, 19] in scope of low-cycle fatigue as

$$D = \int_0^{\hat{\epsilon}^f} m \left(\frac{\bar{\epsilon}^p}{\bar{\epsilon}^f} \right)^{m-1} \frac{\mathrm{d}\bar{\epsilon}^p}{\bar{\epsilon}^f} \tag{4}$$

Here, m is the damage exponent and $\hat{\epsilon}^f$ the equivalent plastic strain for given loading path. The role of damage exponent in the finite element simulations was described in detail by Šebek et al. [20]. The coupling is ensured by weakening functiong w which represents material degradation in accordance to damage accumulation through

$$w = 1 - D^{\beta} \tag{5}$$

There is additional softening parameter β which is the weakening exponent.

The feedback of damage to plasticity is realized through multiplying the original flow stress $\bar{\sigma}_{flow}$ by weakening function as

$$\tilde{\sigma}_{flow} = w\bar{\sigma}_{flow} \tag{6}$$

In the previous equation, $\tilde{\sigma}_{flow}$ is actual flow stress of weakened material or effective stress.

Both aforementioned ductile fracture criteria were developed as uncoupled and were also calibrated with respect to that. Calibration of coupled criteria is very complicated process which requires many computational simulations. Therefore, calibrated fracture envelopes of uncoupled criteria described in previous section were used. The weakening and damage exponents, respectively, were set to have a value of 2 which is widely adopted for metallic materials [21, 22]. This is not a correct calibration procedure which will probably result in premature fracture. Nevertheless, such material constants identification is acceptable for the present paper dealing with slant fracture prediction ability.

3 PREDICTION OF SLANT FRACTURE

3.1 Experiments

Two different specimens were chosen for prediction of slant fracture. The first one is flat specimen loaded by tension which produces slant fracture through the thickness tilted approximately 45 degrees with respect to the major principal stress direction [5, 17, 24, 25]. There is post-mortem specimen of AA 2024-T351 in Fig. 5a. This geometry was overtaken from Bao [17] and used in upcoming numerical simulations. The specimen has 1.6 mm thickness and 50 mm width of the process zone with 8 mm gauge length.

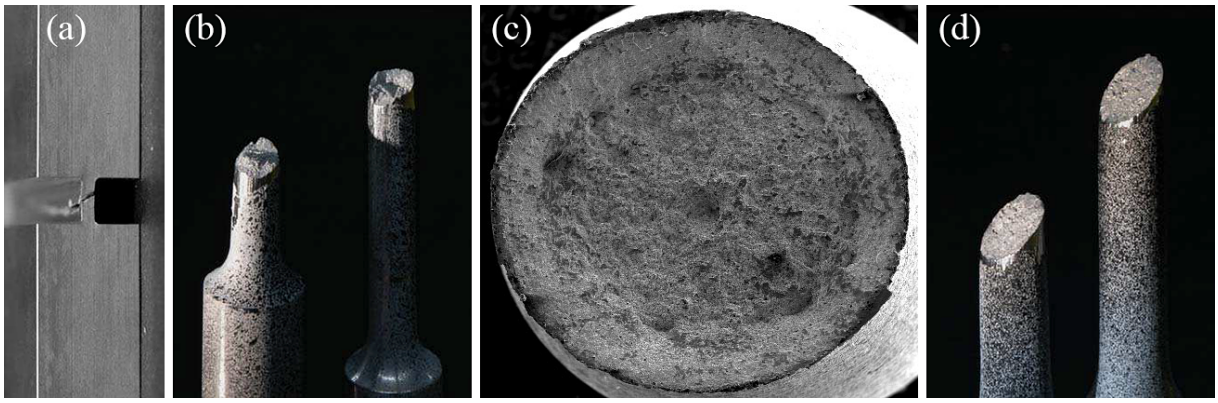

Figure 5: Post-mortem: (a) flat specimen of aluminium alloy 2024-T351 [24]; (b) smooth cylindrical specimen of aluminium alloy 2024-T351 with 6 mm in diameter [24]; (c) smooth cylindrical specimen of AISI 1045 carbon steel [25]; (d) smooth cylindrical specimen of aluminium alloy 2024-T351 with 9 mm in diameter [24].

Another investigated geometry was smooth cylindrical specimen loaded by tension. Typical cup and cone fracture prevails at most metals (Fig. 5b,c). The crack initiation occurs on the axis of symmetry due to void nucleation, growth and coalescence. The crack spreads perpendicularly to the major principal stress, that is perpendicularly to the specimen axis, forming a flat fracture. Then, the nature of mechanism changes to the slant fracture due to increasing shear stress and the crack propagates in the plane of maximum shear stress which is tilted approximately 45 degrees to the specimen axis. Unfortunately, there is often only slant fracture in case of AA 2024-T351 (Fig. 5d) which has still been waiting to be interpreted correctly. Geometry of this specimen was described earlier and used in upcoming numerical simulations.

3.2 Simulations

All numerical simulations were carried out in Abaqus/Explicit commercial finite element code. Fracture criteria were implemented using user subroutine Vectorized User MATerial (VUMAT). Crack initiation and propagation were realized through element deletion technique. Time increment was changed using mass scaling function in order to keep computational time reasonable while retaining negligible ratio of kinetic to internal energy for the whole model.

There was conducted analysis studying the influence of finite elements sizes which were oriented in the loading direction, hereinafter II-orientation, in case of uncoupled criteria. Elements had a size of 0.075, 0.05 and 0.025 mm. Next, there were performed simulations using uncoupled criteria with a mesh of a characteristic element length size of 0.075 mm and finite elements orientation 45 degrees to applied load, hereinafter X-orientation, thus in the direction of supposed crack propagation. Finally, there were conducted computations with elements having size of 0.075 mm with II-orientation for coupled ductile fracture criteria.

3.3 Flat specimen

Only planar model was created in order to save some computational time. It was discretized using 4-node rectangular plane strain elements CPE4R with reduced integration. In case of X-oriented mesh, a negligible amount of 3-node triangular plane strain elements CPE3 was used on lateral sides of the geometry. Areas lying far from the process zone were discretized by coarse mesh, again, in order to save computational time.

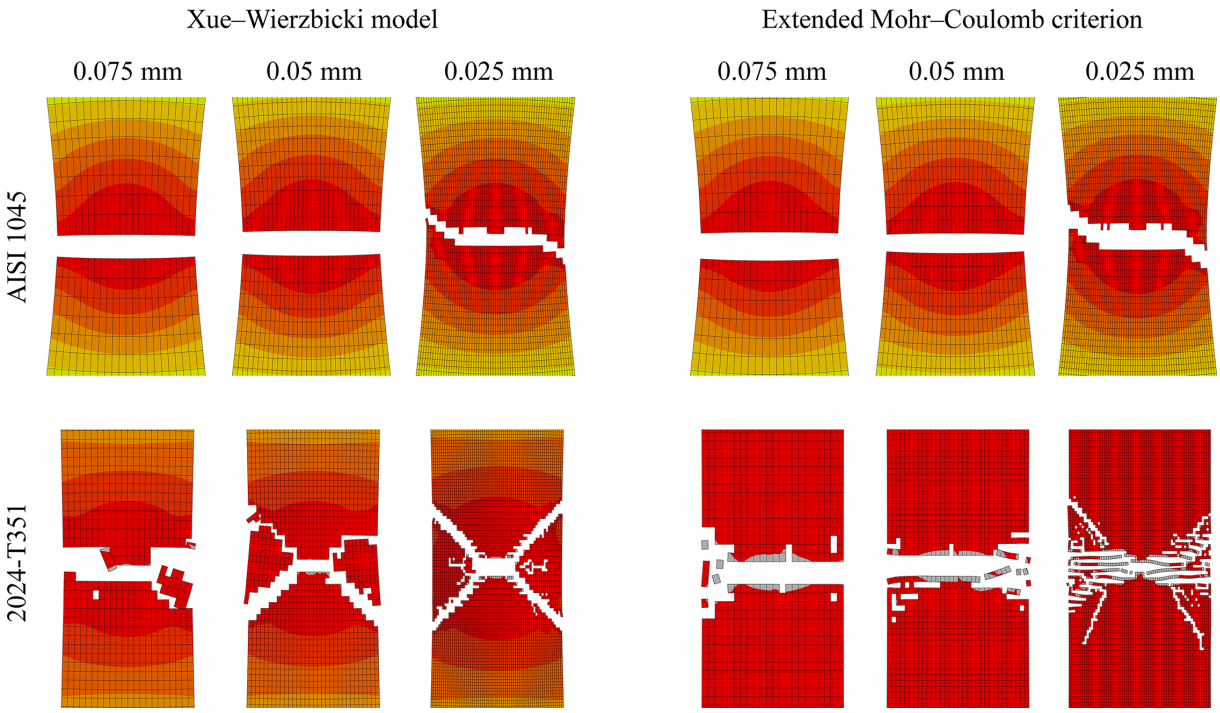

Figure 6: Influence of mesh size for uncoupled fracture criteria and flat specimen with II-orientation.

There is damage parameter in Fig. 6 immediately after the final fracture and separation of the specimen into more pieces for uncoupled criteria and flat specimen with II-orientation. The legend is not shown hereinafter but it was set from 0 to 1 and linearly divided into 20 discrete rainbow contours. The blue colour represents 0 and the red one corresponds to 1.

Both uncoupled criteria are capable of prediction the slant fracture in case of both materials for the mesh with 0.075 mm characteristic element length size.

Models behave similarly in case of AISI 1045 carbon steel, as depicted in Fig. 6. Both meshes with element sizes 0.075 and 0.05 mm, respectively, produce a flat fracture. In case of 0.025 mm, the crack propagates perpendicularly to loading and form a slant fracture in the final stage. There is no splitting into two directions. This is probably due to greater influence of imperfection because there is higher necking than in case of aluminium alloy.

The finer the mesh in case of Xue–Wierzbicki model and 2024-T351, the better the ability to produce the slant fracture. The simulation with size of 0.025 mm predicted the slant fracture very well. Extended Mohr–Coulomb criterion showed similar behaviour but there was huge amount of deleted elements in the perpendicular direction to applied load. This was probably due to fact that, among others, there was higher localization of damage parameter in case of Xue–Wierzbicki model. Crack created X-shaped fracture due to vertical symmetry of the model.

The crack initiation was in the centre of the specimen thickness, in the intersection of all planes of symmetry, for both materials and fracture criteria, respectively, which is in accordance with experimental testing. The slant fractures, which occurred, were 45 degrees to the applied load which is also in good agreement with experiments.

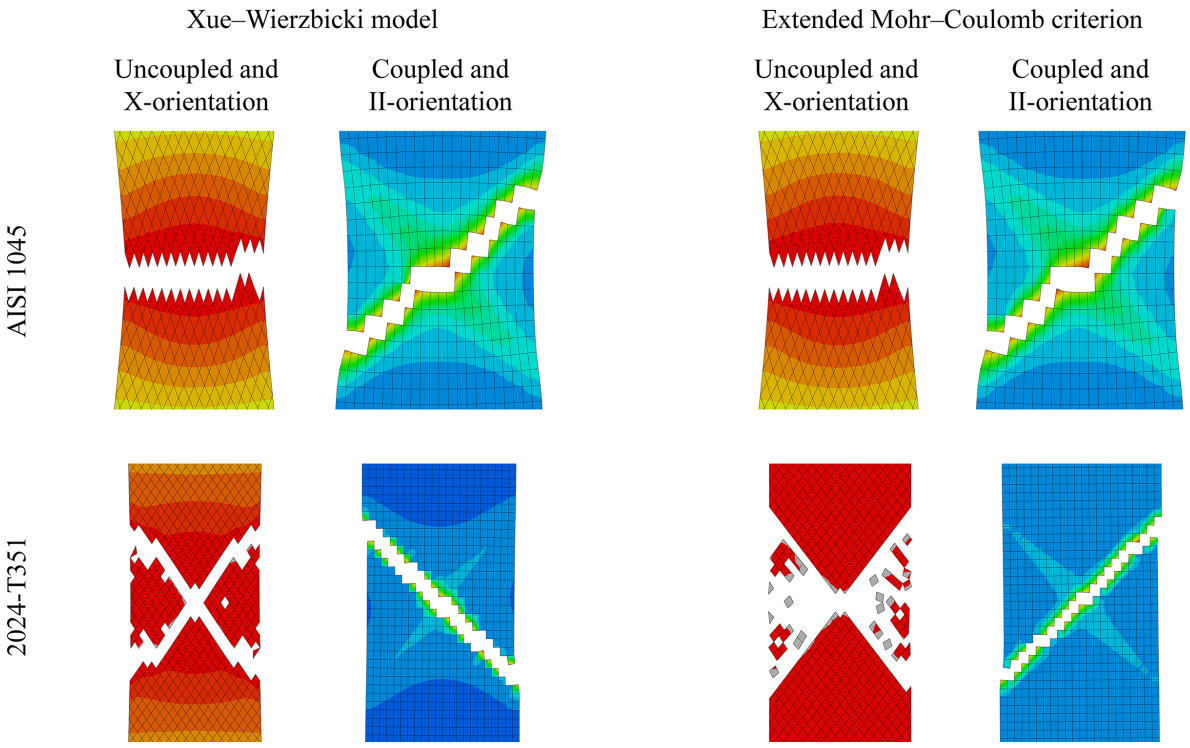

Figure 7: Prediction by uncoupled and coupled criteria for flat plate with X- and II-orientation, respectively.

It is obvious that criteria are capable to predict the slant fracture even with element size of 0.075 mm for X-orientation of the mesh in case of aluminium alloy as in Fig. 7. There is huge amount of deleted elements in case of Extended Mohr–Coulomb criterion, again. Coupled criteria predict the slant fracture without splitting into two direction and propagation of two cracks. Regarding these models, there is a rapid increase of equivalent plastic strain due to softening in the final stage just before crack initiation. This leads to localization of damage parameter and the imperfections play more significant role than in uncoupled models.

The X-orientation, the diagonal one, with characteristic element size of 0.075 mm leads to flat fracture for AISI 1045 (Fig. 7). This mechanism does not change even with using elements of 0.025 mm size. On the other hand, coupled criteria predict slant fracture similarly as in case of AA 2024-T351.

Finally, it is obvious that neither the crack initiation nor the angle of slant crack propagation were influenced by the mesh configuration or coupling the damage with plasticity.

3.4 Smooth cylindrical specimen

Similarly as in previous case, the model was created as axisymmetrical in order to save computational time. The geometry was discretized by 4-node rectangular axisymmetric elements CAX4R with reduced integration. In case of X-oriented mesh, there were used a small number of 3-node triangular axisymmetric elements CAX3 which were located on the axis and on the outer surface of the specimen. The regions outside the process zone were discretized by coarse mesh, again because of saving the computational time, because the deformation and fracture are concentrated into certain section.

Similarly as in case of flat specimen, both models were not capable to describe the slant fracture for both materials and element size 0.075 mm as depicted in Fig. 8.

In case of carbon steel, there was predicted flat fracture independently on the criterion or mesh size.

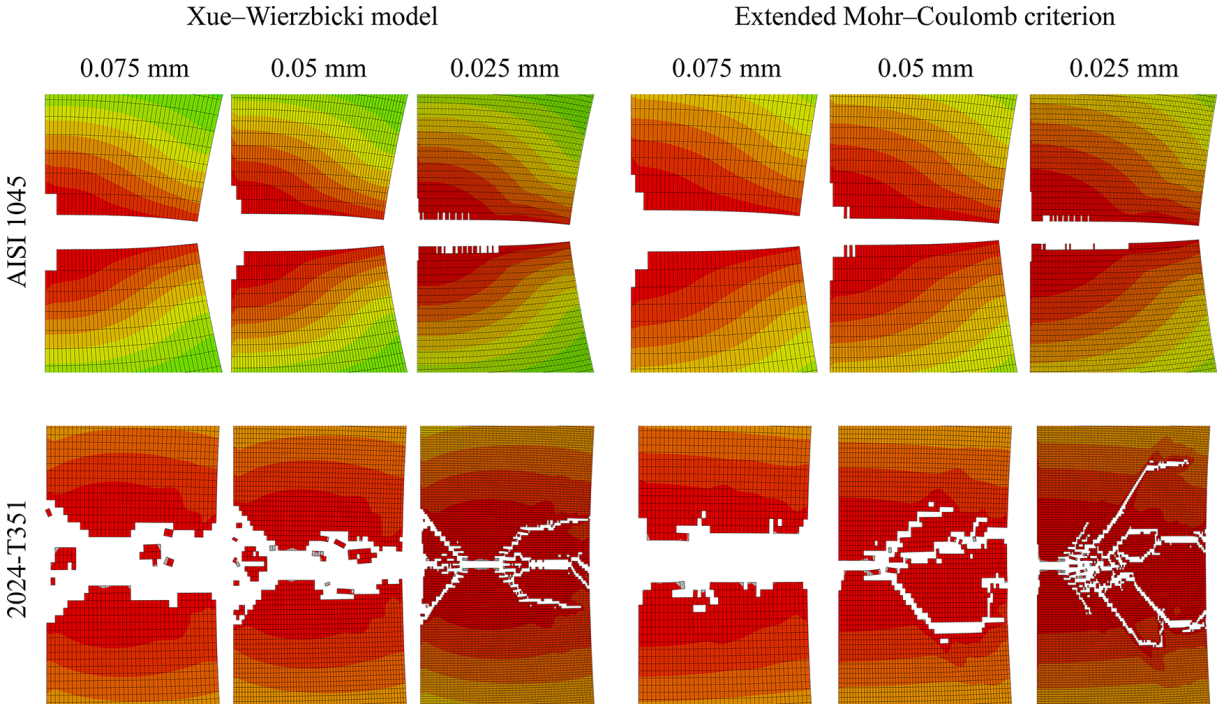

Figure 8: Influence of mesh size for uncoupled fracture criteria and smooth round specimen with II-orientation.

Xue–Wierzbicki model predicted the crack initiation not on the axis of symmetry but in a certain distance towards the outer surface for aluminium alloy which is in contradiction with experiments. Both criteria predicted the flat as well as slant fracture for 0.025 mm sized elements. The slant fracture propagated 45 degrees to applied load at first and then it changed the direction perpendicularly to specimen axis. Extended Mohr–Coulomb criterion exhibited this behaviour also in case of the finite element size of 0.05 mm.

Both uncoupled models with X-oriented mesh produced a flat fracture for carbon steel as in Fig. 9. This behaviour did not change even with decreasing the element size. Coupled Xue–Wierzbicki model produced only flat fracture while coupled Extended Mohr–Coulomb criterion predicted a slight slant fracture in the final stage close to the specimen surface without bifurcation of the crack. In case of 0.05 mm sized finite elements, both coupled models predicted slant fracture in greater distance from the surface in the final stage.

Uncoupled criteria with X-orientation and 0.075 mm sized mesh behaved for the aluminium alloy 2024-T351 the same as in case of II-orientation and 0.025 mm sized finite elements. There was better prediction of crack initiation after coupling the Xue–Wierzbicki model. The crack initiated on the axis of symmetry and there was crack bifurcation in the final stage of rupture governed by shear mechanism. Coupled Extended Mohr–Coulomb criterion predicted slight slant fracture in the final stage. Again, there was significant number of elements deleted in the plane perpendicular to the axis.

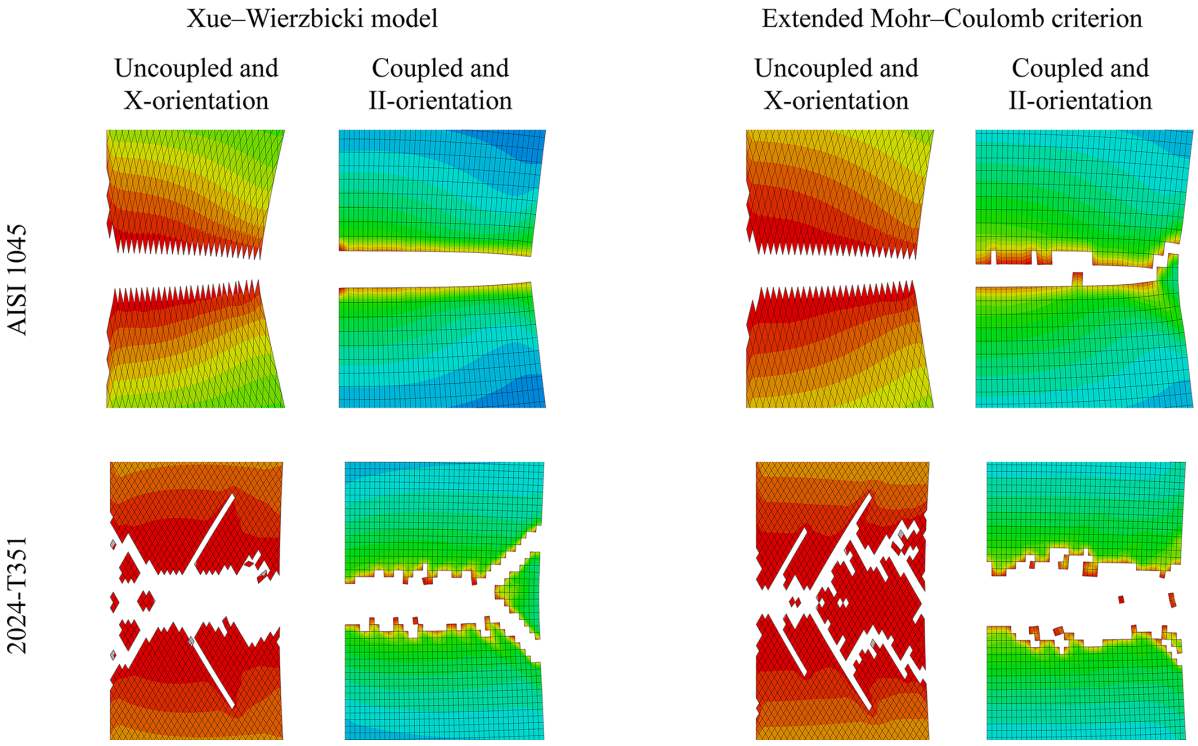

Figure 9: Results of uncoupled and coupled criteria for smooth specimen with X- and II-orientation, respectively.

4 CONCLUSIONS

The present paper was aimed to slant fracture prediction ability of two coupled and uncoupled ductile fracture criteria, originally phenomenological or empirical, Xue–Wierzbicki model and Extended Mohr–Coulomb criterion, for two different metals, aluminium alloy 2024-T351 and AISI 1045 carbon steel. There was conducted analysis studying the influence of the size and orientation of finite element mesh in case of uncoupled criteria. It might be generally stated that the mesh oriented in the direction of applied load exhibited similar results as a finite element mesh oriented in the supposed direction of slant fracture propagation, 45 degress to the applied load in the plane of maximum shear stress, but for much smaller element sizes.

Results also suggest that coupled models are very convenient for slant fracture prediction which is in accordance with recent literature [26, 27]. Such models describe best the real material behaviour. Nevertheless, there is a disadvantage in complex calibration procedure from the perspective of time consumption, high number of experiments needed or complicated implementing and debugging.

5 ACKNOWLEDGEMETNT

This work is an output of project NETME CENTRE PLUS (LO1202) created with financial support from the Ministry of Education, Youth and Sports under the "National Sustainability Programme I".

REFERENCES

[1] L. Xue, W. Mock, T. Belytschko, Penetration of DH-36 steel plates with and without polyurea coating. *Mechanics of Materials*, **42**, 981–1003, 2010.

[2] Y. Li, M. Luo, J. Gerlach, T. Wierzbicki, Prediction of shear-induced fracture in sheet metal forming. *Journal of Materials Processing Technology*, **210**, 1858–1869, 2010.

[3] J. Petruška, P. Kubík, J. Hůlka, F. Šebek, Ductile fracture criteria in prediction of chevron cracks. *Advanced Materials Research*, **716**, 653–658, 2013.

[4] P. Kubík, F. Šebek, J. Hůlka, J. Petruška, Calibration of ductile fracture criteria at negative stress triaxiality. *International Journal of Mechanical Sciences*, **108–109**, 90–103, 2016.

[5] H. Huang, L. Xue, Prediction of slant ductile fracture using damage plasticity theory. *International Journal of Pressure Vessels and Pipping*, **86**, 319–328, 2009.

[6] T.F. Morgeneyer, J. Besson, Flat to slant ductile fracture transition: Tomography examination and simulations using shear-controlled void nucleation. *Scripta Materialia*, **65**, 1002–1005, 2011.

[7] Y. Li, T. Wierzbicki, Prediction of plane strain fracture of AHSS sheets with post-initiation softening. *International Journal of Solids and Structures*, **47**, 2316–2327, 2010.

[8] P.W. Bridgman, *Studies in large plastic flow and fracture: With special emphasis on the effects of hydrostatic pressure*. Harvard University Press, Cambridge, Massachusetts, 1964.

[9] G. La Rosa, G. Mirone, A. Risitano, Postnecking Elastoplastic Characterization: Degree of Approximation in the Bridgman Method and Properties of the Flow-Stress/True-Stress Ratio. *Metallurgical and Materials Transactions A*, **34A**, 615–624, 2003.

[10] G. Mirone, A new model for the elastoplastic characterization and the stress–strain determination on the necking section of a tensile specimen. *International Journal of Solids and Structures*, **41**, 3545–3564, 2004.

[11] T. Wierzbicki, Y. Bao, Y.-W. Lee, Y. Bai, Calibration and evaluation of seven fracture models. *International Journal of Mechanical Sciences*, **47**, 719–743, 2005.

[12] Y. Bai, T. Wierzbicki, Application of extended Mohr–Coulomb criterion to ductile fracture. *International Journal of Fracture*, **161**, 1–20, 2010.

[13] Y. Bai, T. Wierzbicki, A new model of metal plasticity and fracture with pressure and Lode dependence. *International Journal of Plasticity*, **24**, 1071–1096, 2008.

[14] P. Kubík, F. Šebek, J. Petruška, J. Hůlka, J. Růžička, M. Španiel, J. Džugan, A. Prantl, Calibration of selected ductile fracture criteria using two types of specimens. *Key Engineering Materials*, **592–593**, 258–261, 2014.

[15] F. Šebek, P. Kubík, J. Petruška, Chevron crack prediction using the extremely low stress triaxiality test. *MM Science Journal*, 617–621, 2015.

[16] F. Šebek, P. Kubík, J. Hůlka, J. Petruška, Strain hardening exponent role in phenomenological ductile fracture criteria. *European Journal of Mechanics - A/Solids*, **57**, 149–164, 2016.

[17] Y. Bao, *Prediction of ductile crack formation in uncracked bodies*. PhD thesis, Massachusetts Institute of Technology, 2003.

[18] L. Xue, Damage accumulation and fracture initiation in uncracked ductile solids subject to triaxial loading. *International Journal of Solids and Structures*, **44**, 5163–5181, 2007.

[19] L. Xue, A unified expression for low cycle fatigue and extremely low cycle fatigue and its implication for monotonic loading. *International Journal of Fatigue*, **30**, 1691–1698, 2008.

[20] F. Šebek, J. Hůlka, P. Kubík, J. Petruška, On the Proportionality of Damage Rule in Finite Element Simulations of the Ductile Failure. *Advanced Materials Research*, **980**, 189–193, 2014.

[21] B.L. Boyce, S.L.B. Kramer, H.E. Fang, T.E. Cordova, M.K. Nielsen, K. Dion, et al., The Sandia Fracture Challenge: blind round robin predictions of ductile tearing. *International Journal of Fracture*, **186**, 5–68, 2014.

[22] T.S. Cao, *Modeling ductile damage for complex loading paths*. PhD thesis, École Polytechnique Université, 2013.

[23] T.S. Cao, Numerical simulation of 3D ductile cracks formation using recent improved Lode-dependent plasticity and damage models combined with remeshing. *International Journal of Solids and Structures*, **51**, 2370–2381, 2014.

[24] L. Xue, *Ductile Fracture Modeling - Theory, Experimental Investigation and Numerical Verification*. PhD thesis, Massachusetts Institute of Technology, 2007.

[25] J. Bořkovec, *Computer simulation of material separation process*. PhD thesis, Brno University of Technology, 2008.

[26] X. Teng, Numerical prediction of slant fracture with continuum damage mechanics. *Engineering Fracture Mechanics*, **75**, 2020–2041, 2008.

[27] G. Rousselier, M. Luo, A fully coupled void damage and Mohr–Coulomb based ductile fracture model in the framework of a Reduced Texture Methodology. *International Journal of Plasticity*, **55**, 1–24, 2014.